ELSEVIER

Marine Geology 225 (2006) 145–156

MARINE GEOLOGY
INTERNATIONAL JOURNAL OF MARINE GEOLOGY, GEOCHEMISTRY AND GEOPHYSICS

www.elsevier.com/locate/margeo

Hydrothermal manganese oxide deposits from Baby Bare seamount in the Northeast Pacific Ocean

C.E. Fitzgerald, K.M. Gillis *

School of Earth and Ocean Sciences, University of Victoria, P.O. Box 3055 Station CSC, Victoria, British Columbia, Canada V8W 5C2

Received 9 June 2005; received in revised form 12 August 2005; accepted 1 September 2005

Abstract

Manganese oxide crusts were recovered from Baby Bare seamount in order to investigate the history of off-axis hydrothermal venting. Baby Bare is a small basement high protruding from a regional sediment cover on the eastern flank of the Juan de Fuca Ridge that acts as a focus for discharging crustal fluids. Stratabound Mn-oxide crusts were collected where warm venting has been observed near the seamount summit. Mn-oxide crusts are composed primarily of 10 Å manganate ± pyrolusite, with minor nontronite, saponite, and/or barite. These assemblage and chemical characteristics such as high Mn/Fe ratios and low trace metal and REE concentrations are indicative of a hydrothermal origin. Minimum ages for these deposits, calculated using growth rates (324 to ~1800 mm/Ma) and estimated thicknesses of manganese outcrops, show that Baby Bare has been hydrothermally active for at least 0.5 Myr, and possibly since its formation (1.7–2.7 Ma). Hydrothermal manganese oxide crusts such as these from Baby Bare record interactions between the hydrothermal fluids and seawater and are important tools for estimating the longevity of off-axis hydrothermal activity.

Keywords: hydrothermal; manganese oxide; Baby Bare seamount; off-axis hydrothermal circulation; Juan de Fuca eastern flank

1. Introduction

Circulation of seawater through basaltic ocean crust is one of the largest geochemical cycles on earth and significantly alters the chemical and biological states of the crust and oceans. In the ridge-flank environment, seawater convection is driven by heat associated with cooling of the lithosphere. It may persist for millions of years and accounts for 20% of the total heat flux through the seafloor (Stein and Stein, 1994; Elderfield and Schultz, 1996; Mottl et al., 1998). Basement topographic highs and seamounts are common features on flanks (Wessel, 2001; Villinger et al., 2002) and may act as sites for crustal fluid discharge (Mottl and Wheat, 1994; Mottl et al., 1998; Wheat and McDuff, 1995) or recharge (Fisher et al., 2003). Venting of low temperature, chemically modified seawater at discharge sites commonly results in the accumulation of hydrothermal deposits (e.g., Honnorez et al., 1983; Alt, 1988) and development of vent-associated faunal communities (Mottl et al., 1998).

Baby Bare seamount, located on the east flank of the Juan de Fuca Ridge (Fig. 1A), is one of several isolated outcrops that rises above the regionally continuous sediment cover of the Cascadia Basin (Becker et al., 2000). The turbiditic sedimentary fill effectively seals the basin, limiting hydrological and geochemical ex-

* Corresponding author. Tel.: +1 250 472 4345; fax: +1 250 721 6200.
E-mail addresses: kcfitz@telus.net (C.E. Fitzgerald), kgillis@uvic.ca (K.M. Gillis).

0025-3227/$ - see front matter © 2005 Elsevier B.V. All rights reserved.
doi:10.1016/j.margeo.2005.09.005

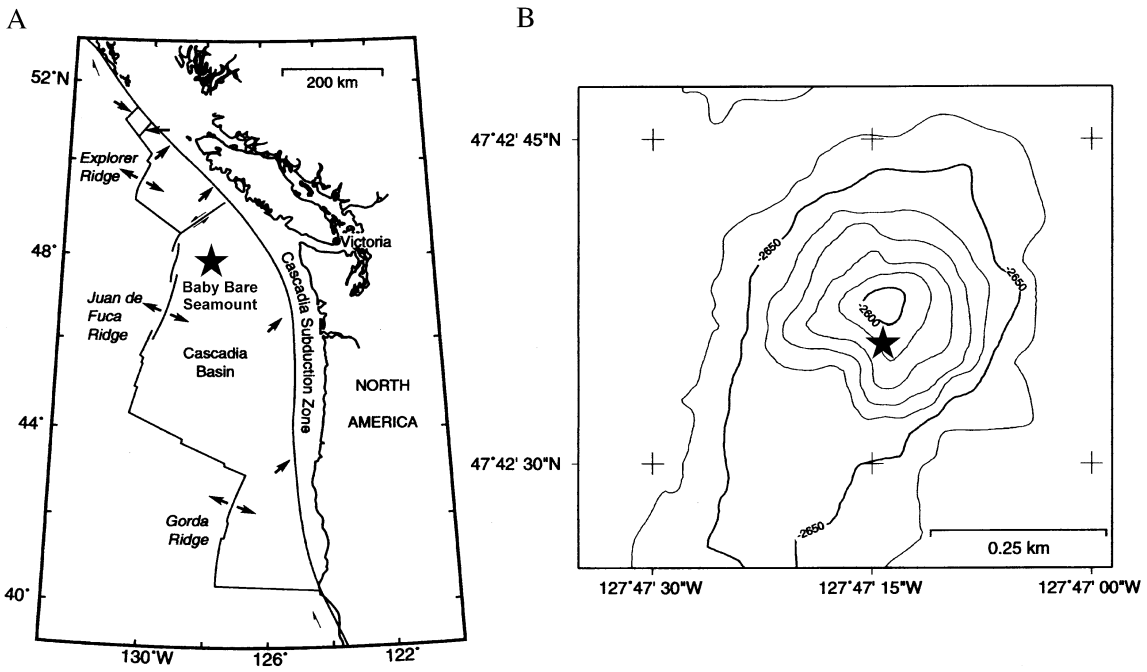

Fig. 1. (A) Location of Baby Bare seamount on the eastern flank of the Juan de Fuca Ridge in the Northeast Pacific Ocean. (B) Location of natural warm springs observed in 1998 and the area of Mn-oxide crust sampling near the summit of Baby Bare seamount (Becker et al., 2000).

change between the volcanic crust and ocean, except in the vicinity of exposed edifices where large heat flow and geochemical anomalies are observed (Davis et al., 1992; Mottl and Wheat, 1994; Becker et al., 2000). These edifices facilitate fluid flow between the volcanic basement and ocean, serving both as discharge sites for warm, spring fluids (e.g., Baby Bare seamount) and recharge sites for unmodified seawater (e.g., Grizzly Bare seamount) (Wheat et al., 2002; Fisher et al., 2003). At the summit of Baby Bare seamount, Mn oxides have accumulated in the vicinity of warm venting fluids and vent fauna communities (Mottl et al., 1998; Becker et al., 2000). In this paper, we present the results of a mineralogical and geochemical study of Mn-oxide deposits from Baby Bare seamount. We confirm the prediction of Wheat and Mottl (2000) that the deposits are hydrothermal in origin and show that spring fluid chemistry and hydrothermal mineral assemblages control the Mn-oxide compositions. We predict that Baby Bare seamount has served as a discharge site for at least 0.5 Myr, and perhaps since its formation.

2. Regional setting and sample suite

Baby Bare seamount is the southernmost of three basement highs located along a linear basement ridge produced by volcanic and tectonic processes at the Juan de Fuca Ridge ~3.5 Myr ago (Kappel and Ryan, 1986; Davis et al., 1997). The eastern flank of the Juan de Fuca Ridge is buried by continentally derived Pleistocene turbiditic and hemipelagic sediments that form a flat-lying plain known as the Cascadia Basin (Davis et al., 1992). These sediments are composed of quartz and clay minerals such as kaolinite, illite, chlorite and saponite and have low organic contents (<1%) (Underwood and Hoke, 2000; Buatier et al., 2001). Baby Bear seamount rises 70 m above the basin and formed by off-axis volcanism between 1.7 and 2.7 Ma, based on regional sediment thickness and fossil assemblages (Davis et al., 1997; Becker et al., 2000). Hydrothermal discharge at Baby Bare seamount is focused in an area 10–50 m southeast of the summit, along a N to NE trending fault (Mottl et al., 1998) (Fig. 1B). Alvin dives in 1995 discovered warm (25 °C) hydrothermal fluids venting through lava outcrops and a thin (<0.7 m) sediment cover (Mottl et al., 1998). Focused venting was not evident in 2002 and 2003; however, disturbance of sediment released fluids, indicating that the area was still hydrothermally active at the time (Johnson, 2003). This was confirmed by the presence of spider crabs, crinoids, brittle stars, and purple Pacific octopus in 2002/2003 (Johnson, 2003). Regional heat flow and seismic data indicate that the sediment–basement contact is isothermal at ~62–64 °C, which demonstrates that the warm (25 °C) basement fluids cooled conductively in the sediment column (Davis et al.,

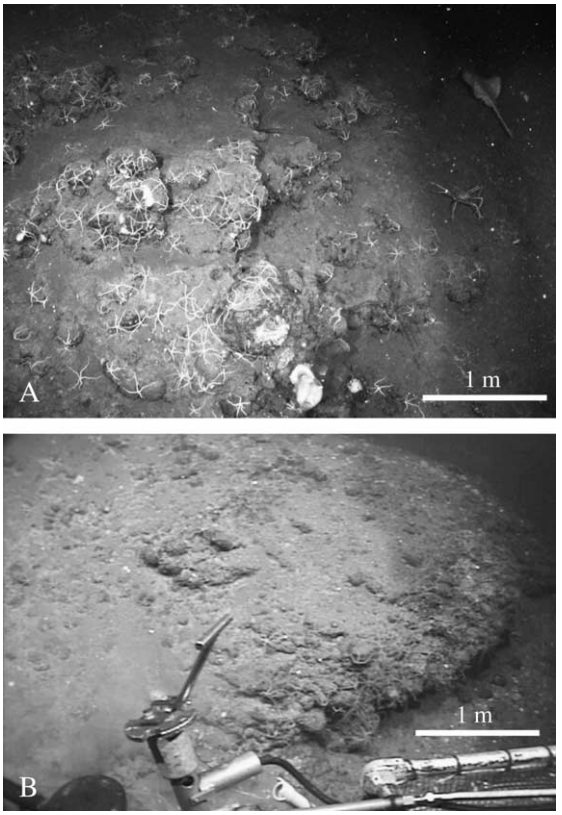

Fig. 2. (A) Bulbous Mn-oxide deposits near the summit of Baby Bare seamount covered by biological organisms, including crabs, crinoids, brittle stars, rays and Pacific octopus. (B) Outcrop of Mn-oxide deposits. Note arm of *ROV Jason* in lower right.

1997; Mottl et al., 1998). Spring (hydrothermal) fluids and pore fluids extracted from sediments onlapping the summit evolved from seawater in the volcanic basement by fluid–rock reactions at moderate temperatures (up to 70 °C) (Davis et al., 1997; Wheat and Mottl, 2000; Wheat et al., 2000). High advection rates (>2–10 cm/yr) through the sediments probably minimized further reaction, although high concentrations of some elements (e.g., Mn, Ni, Zn) in spring fluids are partly attributed to near surface reactions (Wheat and Mottl, 2000; Wheat et al., 2000).

The summit area and upper flanks of Baby Bare seamount are mostly covered by <0.7 m of hemipelagic sediment, with scarce outcrops of basalt (~1% of summit). Mn-oxide layers and crusts up to 0.5 m thick (the extent visible above the sediments) occur in the area of venting (Fig. 2A and B)(Wheat and Mottl, 2000). Fragments of Mn-oxides of varying size (~5 to 30 cm) also lie loosely on top of sediment in some areas. Sediment colour ranged from pale to dark brown on the surface, but appeared grey below the sediment surface. The Mn-oxides are primarily stratabound (Hein et al., 1990), and partially cement the sediments that overlie the summit of Baby Bare.

3. Sample suite

Six Mn-oxide crust samples were recovered from near the summit area where fluids were venting in 1995 (Fig 1B and Table 1). Samples 04-02, 04-03, and 62-04 were broken off Mn-oxide outcrops, whereas samples 05-04, 05-05, and 63-11 were lying loose on or in the sediment. All the crusts were hard and bluish-black to grey-black with a submetallic luster, typical of many hydrothermal manganese crusts (Eckhardt et al., 1997). The crusts were dense with low porosity (<5%). Upper surfaces of the crusts were coated in a thin (<10 mm), discontinuous layer of light brown sediment with patches of biological material. In addition, most samples were coated in a thin (<3 mm), discontinuous and dull Mn-oxide coating that may have been hydrogenous in origin. Small (<1 cm in diameter and thickness) patches of green and yellow clays and orange Fe-oxyhydroxides also formed thin, discontinuous coatings on the upper surfaces of several samples, occurring beneath and intermixed with hydrogenous Mn-oxides. Lower surfaces were coated with a thin (<1 cm) coating of dark brown sediment. Small clumps of light and dark brown clay-like sediments (<5% of samples) were incorporated into the Mn crusts, presumably as the oxide accumulated.

Four samples (04-02, 04-03, 05-04 and 63-11) were massive (Fig. 3A); sample 63-11 has clumps of radiating fibers on fresh interior surfaces and four (<0.5 mm thick) laminations at its base. Two samples (05-05 and 62-04) were laminated and were subdivided for chemical and mineralogical analysis based on texture and colour. Sample 05-05 was divided into two: dark grey massive outer rind (05-05A) and an inner core that consisted of grey clumps of fine radiating needles (05-05B). Sample 62-04 was divided into three sub-

Table 1
Mn-oxide crust sample locations[a]

Sample no.	Depth (m)	Latitude	Longitude
J2-04-02	2596	47 42.596°N	127 47.140°W
J2-04-03	2595	47 42.596°N	127 47.140°W
J2-05-04	2594	47 42.604°N	127 47.135°W
J2-05-05	2591	47 42.615°N	127 47.134°W
J2-62-04	2600	47 42.603°N	127 47.158°W
J2-63-11	2599	47 42.605°N	127 47.151°W

[a] Samples were collected during cruises *R/V Thomas G. Thompson*, Leg 158 in 2002 (Johnson, unpublished cruise report, 2002) and *R/V Atlantis Voyage 7*, Leg 20 in 2003, using the remotely operated vehicle *Jason II*.

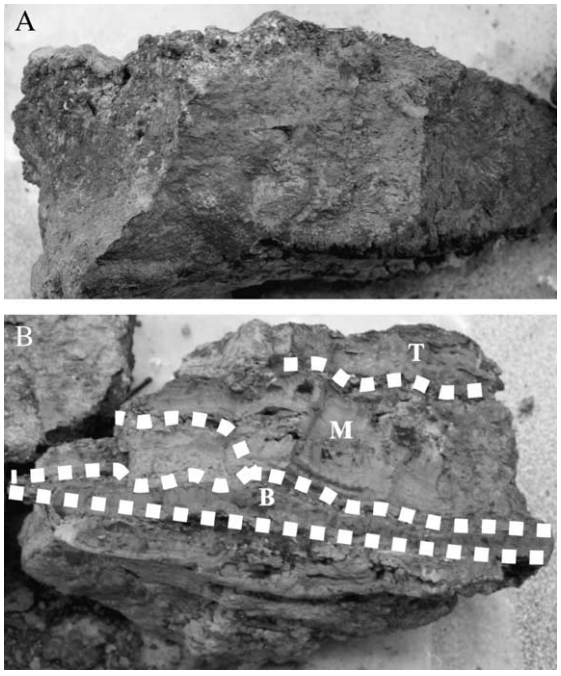

Fig. 3. (A) Massive Mn-oxide crust (sample 63-11). Radiating fibers of 10 Å manganate are visible on the fresh surface. Sample is 7 cm long and 3.5 cm wide. (B) Subdivision of sample 62-04 into three horizons based on textural and colour differences. Sample is 11 cm long and 6 cm wide.

samples (Fig. 3B): ~1 cm top horizon (62-04T) that consisted of 6-10 bluish-black discontinuous laminations <2 mm thick; a grayish-black more massive middle horizon 25 mm thick (62-04M); and a black bottom horizon that had a cusp-like texture and consisted of two laminations <4 mm thick (62-04B). There is no relationship between texture of Mn-oxides and locations on outcrops or sediment.

4. Analytical methods

All Mn crusts were analyzed in bulk, with the exception of 05-05 and 62-04, which were subdivided on the basis of colour and texture (see Section 3). Before samples were crushed, sediment and hydrogenous Mn material on the outer surfaces and sediment incorporated into the crusts during growth were carefully removed. Samples were then ground into a fine powder using a tungsten carbide ring mill and an agate pestle and mortar.

Major elements and selected trace elements (Co, Cu, Ni, V and Zn) were analyzed by X-ray Fluorescence (XRF) with a Philips PW2440 4 kW automated XRF spectrometer at McGill University in Montreal, Québec. Fused beads were prepared from a 1:5 sample/lithium tetraborate mixture. Accuracy is within 0.5% for silica, 1% for other major elements and 5% for trace elements; precision is within 0.5% relative for each element. Accuracy was determined using natural samples and standards. Other trace elements and the rare earth elements (REE) were analyzed by inductively coupled plasma mass spectrometry using a Thermo Instruments PQII ICP–MS with a Gilson® auto-sampler and peristaltic pump at the University of Victoria in Victoria, British Columbia. The dissolution procedure followed the hotplate methods of Taylor et al. (2002), except that HF was added only once during dissolution. Final solutions were mixed to a final weight of 50 g in polycarbonate Falcon tubes using 1% HNO_3 and 1 ml of a complexing agent consisting of 0.11 N HF, 0.45 N boric and 0.22 N oxalic acids. Reproducibility for Sr, Ba, Zr, Na, Cr, Hf, Th, U and most REEs was within 10% (Eu, Tb, Ho, Tm, and Lu were 20–55%) and 14–28% for Sc, V, Cr, Ni, Rb, Cs. Barium occurs in high concentrations in these crusts and has a high oxide bonding energy that causes interferences in the determination of Eu (Dulski, 1994). Eu concentrations were corrected by subtracting the measured $Ba^{16}O$ from the total measured Eu. This resulted in Eu being below detection limits (0.05 ppm) for all samples except 62-04B.

Bulk mineralogy was determined using a Siemens D5000 powder X-ray Diffractometer at the University of British Columbia, in Vancouver. Samples were run at 40 kV, 30 mÅ Cu-Kα with a monochromatized scan from 3° to 50° 2θ and were run glycolated and unglycolated to identify clay minerals.

5. Results

5.1. Mineralogy

Almost all samples are composed primarily of 10 Å manganate, with characteristic X-ray diffraction peaks at 9.6 Å, 4.8 Å and 3.4 Å. Pyrolusite [δ-MnO_2] is a dominant phase in samples 62-04 and 63-11, with peaks at 3.13 Å, 2.41 Å, 2.21 Å, 2.11 Å and 1.98 Å. Minor 10 Å manganate occurs in these samples. Saponite and nontronite occur as minor phases in many crusts (saponite was identified in all samples but 05-05, nontronite in all but 05-04 and 62-04M). Barite was also identified in sample 05-05A and may be present in samples 04-02, 04-03 and 05-04, however, barite identification was inconclusive as the primary barite peaks in these samples were missing or very small. The subdivided sample 62-04B had a slightly larger primary pyrolusite peak and smaller primary 10 Å manganate peak than 62-04T and 62-04M.

It is notable that XRD and TEM data have confirmed the presence of todorokite (10 Å manganate) in Mn crusts from other seamounts in the area (Buatier et al., 2004). We therefore propose that the common mineral assemblage of Mn-oxide crusts at Baby Bare seamount is todorokite ± pyrolusite ± saponite ± nontronite. This assemblage has been documented for other seamount-hosted Mn-oxide deposits, such as the Bonin (Usui et al., 1986) and Yap (Hein et al., 1992a) arcs.

5.2. Bulk chemistry

Baby Bare Mn-oxide crusts show a range in major element compositions (Table 2). Mn and Fe concentrations range from ~39 to 54 wt.% and ~1.7 to 2.6 wt.%,

Table 2
Major element (wt.%) and trace element (ppm) chemistry with Mn/Fe and Si/Al ratios for Mn-oxide crusts recovered from Baby Bare seamount

Sample no.	J2-04-02	J2-04-03	J2-05-04	J2-05-05a	J2-05-05b	62-04T	62-04M	62-04B	63-11
Analysis	Bulk	Bulk	Bulk	Rind	Core	Top	Middle	Bottom	Bulk
Si	4.52	2.82	5.52	0.67	0.28	1.67	1.23	1.05	0.39
Ti	0.09	0.06	0.02	<d/l	<d/l	0.03	0.02	0.01	<d/l
Al	0.83	0.58	0.17	0.11	0.03	0.31	0.22	0.17	0.05
Fe	2.59	2.29	5.80	0.91	1.71	1.94	1.87	1.88	1.69
Mn	43.35	46.22	39.60	51.70	54.32	47.54	50.26	50.87	52.85
Mg	1.83	1.93	1.59	1.60	1.23	1.69	1.78	1.54	1.03
Ca	1.18	1.04	1.01	1.14	1.17	0.87	0.87	0.85	0.59
Na	0.88	0.76	0.77	0.68	0.55	0.67	0.66	0.57	0.20
K	0.55	0.34	0.42	0.07	0.05	0.21	0.17	0.10	0.04
P	0.03	0.04	0.02	0.03	0.05	0.04	0.03	0.04	0.06
LOI	19.02	20.22	20.66	21.01	19.63	23.71	21.77	22.15	24.83
Mn/Fe	16.75	20.14	6.83	27.07	31.69	24.53	26.80	27.05	31.22
Si/Al	5.46	4.86	32.57	6.36	9.63	5.36	5.47	6.02	7.72
Cr	15	25	8	4	7	10	4	4	3
Ba	2489	8109	5466	11412	15999	5799	5344	6345	2862
Cu	37	1141	192	106	59	187	74	150	88
Ni	212	967	79	227	156	329	208	354	174
Zn	0	375	0	85	161	128	6	98	256
Co	81	126	88	115	151	138	157	262	100
V	85	463	104	47	112	231	117	159	233
Sc	3	2	<d/l	<d/l	3	1	<d/l	2	<d/l
Rb	38	18	18	11	8	13	9	10	3
Sr	706	576	666	987	1154	959	778	1138	933
Y	6	12	5	6	14	16	6	14	11
Zr	12	27	4	5	3	14	4	11	3
Nb	2	2	<d/l	<d/l	<d/l	1	<d/l	1	<d/l
Cs	3	1	1	<d/l	<d/l	1	<d/l	<d/l	<d/l
La	4	14	3	3	5	10	4	9	6
Ce	8	10	4	3	<d/l	6	3	6	4
Pr	1	3	1	1	1	2	1	2	1
Nd	4	12	3	3	3	9	3	9	5
Sm	1	3	1	1	1	2	1	2	1
Eu	<d/l	<d/l	<d/l	<d/l	<d/l	<d/l	<d/l	0	<d/l
Gd	1	3	1	1	1	3	1	2	2
Tb	<d/l	<d/l	<d/l	<d/l	<d/l	<d/l	<d/l	<d/l	<d/l
Dy	1	3	1	1	1	3	1	2	2
Ho	<d/l	1	<d/l	<d/l	<d/l	1	<d/l	<d/l	<d/l
Er	1	2	<d/l	<d/l	1	2	1	2	1
Tm	<d/l	<d/l	<d/l	<d/l	<d/l	<d/l	<d/l	<d/l	<d/l
Yb	1	2	0	1	2	2	1	1	1
Lu	<d/l	<d/l	<d/l	<d/l	<d/l	<d/l	<d/l	<d/l	<d/l
Hf	<d/l	<d/l	<d/l	<d/l	<d/l	<d/l	<d/l	<d/l	<d/l
Ta	<d/l	<d/l	<d/l	<d/l	<d/l	<d/l	<d/l	<d/l	<d/l
Th	1	1	<d/l	<d/l	<d/l	1	<d/l	<d/l	<d/l
U	2	3	1	1	3	7	7	8	10

<d/l = concentrations were less than detection limits.

respectively. Mn and Fe are highly fractionated, with Mn/Fe ratios ranging from ~7 to 32. Si and Fe are slightly higher in samples 04-02, 04-03 and 05-04, probably due to the incorporation of minor amounts of nontronite and/or saponite. This interpretation is supported by XRD data that show the strongest peaks for nontronite and/or saponite for these samples. Ca, Na, K, and Mg contents are <2 wt.%. Si/Al ratios generally range from ~4 to 9, similar to the ratio of the hemipelagic sediments (~1 to 6.5) collected from ODP hole 1026C drilled close to the Baby Bare edifice (Buatier et al., 2001).

Trace metal (Cu, Co, Ni, and Zn) concentrations are typically <1000 ppm. Ba shows the greatest variation (~2400 to ~16,000 ppm); sample 05-05, which contains barite as a minor phase, has the highest Ba concentrations (Table 2). Concentrations of other trace elements, such as V, Y, Zr, U, and Th, are low (Table 2), and crusts have variable Co/Zn ratios (0.3–1.35).

Total REE concentrations are low, with ΣREE ranging from ~13 to 52 ppm. Chondrite-normalized REE patterns display LREE-enrichment with La_N/Sm_N ratios ranging from 2.7 to 4.3 and Dy_N/Yb_N ranging from 0.4 to 1.1. The crusts exhibit prominent negative Ce anomalies ($Ce_N/Ce_N^* = Ce_N/10^{(\log La_N + \log Pr_N)/2)}$), with values ranging from 0.32 to 0.96, and negative Eu anomalies (Fig. 4).

Of the subdivided samples, sample 05-05A has slightly higher Cu and Ni concentrations and slightly less Ba, Zn and Co concentrations than 05-05B. Of the three horizons analyzed for sample 62-04, the top and bottom are more alike than the middle. Concentrations of Ba, Cu, Ni, Zn, Co, V, Rb, Y, Zr, Nb, and REEs are slightly higher in the top and bottom sections than in the middle.

6. Discussion

6.1. Classification as hydrothermal crusts

Manganese-oxide deposits occur in many tectonic settings throughout the world ocean. They may be classified as hydrogenous, diagenetic and hydrothermal in origin, based on mineralogy, chemical composition and tectonic setting (Hein et al., 1997). Hydrogenous crusts precipitate slowly (2–10 mm/Myr), from seawater in the form of crusts or pavements, precipitating on sediment-free, hard substrates (Halbach et al., 1983; Manheim and Lane-Bostwick, 1988; Ingram et al., 1990). They are primarily composed of poorly crystalline manganese oxide (δ-MnO_2 or vernadite) and amorphous iron oxyhydroxides. These crusts have Mn/Fe ratios of ~1, high concentrations of Ni and Cu (>3000 ppm) and REE concentrations, and positive Ce anomalies (Toth, 1980; Bolton et al., 1988; Ingram et al., 1990; Usui and Nishimura, 1992; Hein et al., 1996, 1997; Usui and Someya, 1997). Diagenetic deposits typically form nodules that precipitate slowly (<100 mm/Myr) from diagenetically altered sediment pore waters away from hydrothermal sources (Calvert and Price, 1970; Bonatti et al., 1972; Klinkhammer et al., 1982; Manheim and Lane-Bostwick, 1988). Hydrothermal Mn-oxide deposits precipitate directly from low-temperature hydrothermal fluids at rates typically

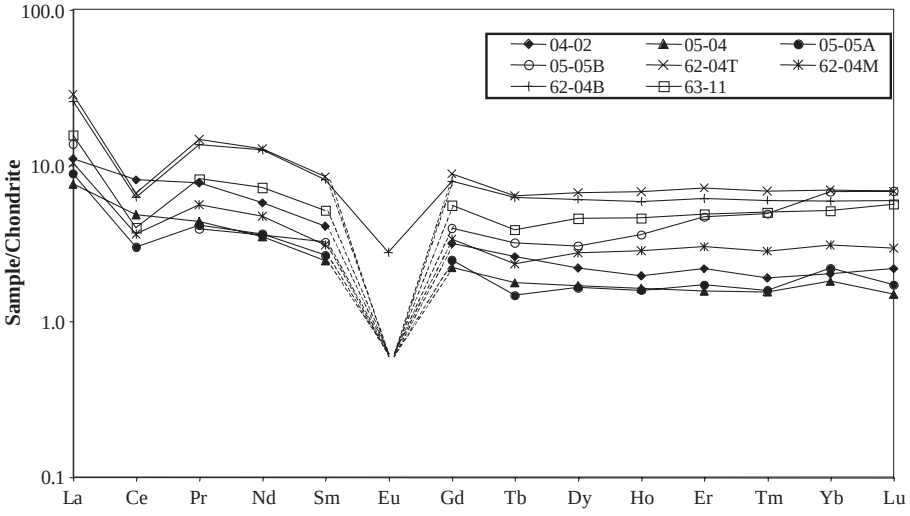

Fig. 4. Chondrite-normalized rare earth element plot for Mn-oxide crusts from Baby Bare seamount (chondritic values from Sun and McDonough, 1989). All samples except 04-02 and 05-04 have pronounced negative Ce anomalies; sample 62-04B also has a strong negative Eu anomaly. Eu in all other samples is below detection limits (0.05 ppm); note that dashed lines indicate the value for the detection limit for Eu.

>1000 mm/Myr (Ingram et al., 1990; Hein et al., 1997). These deposits usually have a laminated texture and are stratabound (cementing sediment) (Hein et al., 1997). Both diagenetic and hydrothermal crusts are composed of 10 Å and/or 7 Å manganate, have high Mn/Fe ratios (>10) and low trace metal contents (Cronan et al., 1982; Bolton et al., 1988; Varentsov et al., 1991; Usui and Nishimura, 1992; Hein et al., 1994, 1996). Because of similarities between these two types of crusts, they are usually distinguished based on crust morphology, tectonic setting and growth rate (Varnavas et al., 1988; Kuhn et al., 1998).

Manganese-oxide crusts from Baby Bare are first classified based on the relative abundance of Mn, Fe and selected trace elements. On the conventional ternary diagram of Mn–Fe–(Co+Ni+Cu)×10 (Bonatti et al., 1972), Baby Bare crusts plot in the high Mn field, where the diagenetic and hydrothermal fields overlap (Fig. 5A). The ternary diagram of Toth (1980) distinguishes hydrothermal and diagenetic sources and points to a hydrothermal origin for the Baby Bare samples (Fig. 5B). Three samples trend towards the diagenetic field, reflecting either a diagenetic influence or, more probably, the incorporation of clay minerals into the samples during growth.

Textural evidence also points to a hydrothermal origin. The layered structure of these crusts is common in hydrothermal oxide deposits, reflecting variation in intensity of hydrothermal discharge (Lalou, 1983) or changes in the pH and/or redox conditions during growth of the crusts (Eckhardt et al., 1997). The stratabound nature of the crusts is also consistent with a hydrothermal origin (Hein et al., 1997).

In summary, chemical, mineralogical and textural properties, and the tectonic setting of Baby Bare indicate that the Mn-oxide crusts formed by hydrothermal processes. In particular, the chemistry of the Mn-oxides is consistent with average chemical compositions of hydrothermal crusts collected in other tectonic settings, such as those found at volcanic arcs (Cronan et al., 1982; Bolton et al., 1988; Hein et al., 1990), back arc spreading centers (Halbach et al., 1989; Herzig et al., 1990), midplate hot-spot volcanoes (DeCarlo, 1983; Hein et al., 1996) and mid-ocean ridges (Grill et al., 1981).

6.2. Elemental sources and growth conditions

Classification of the Baby Bare Mn-oxide crusts as hydrothermal implies formation by precipitation from warm fluids within and on top of the sediment near the summit of the seamount, as predicted by Wheat and Mottl (2000). Spring fluids are mixtures of upwelling basement fluids and seawater that vented directly from basalt or through a thin (<0.7 m) sediment carapace (Mottl et al., 1998; Wheat and Mottl, 2000; Wheat et al., 2002). All spring fluids are Mn-enriched relative to seawater, as a result of reactions occurring within the volcanic sequence. Fluids venting through sediment are slightly more Mn-enriched, due to microbially mediated processes at or near the seafloor (Wheat and Mottl, 2000). Similarly, Co, Ni, and Zn are slightly more enriched in fluids venting through sediment versus basalt and in spring fluids relative to seawater (Wheat et al., 2002). Mn and Fe are probably fractionated during the hydrothermal process resulting in the deposition of Fe, as sulfides in the ocean crust, and of Mn, as Mn-oxide crusts at the seafloor.

Discharging reduced warm spring fluids are mixed with oxygenated seawater at or near the seawater–sed-

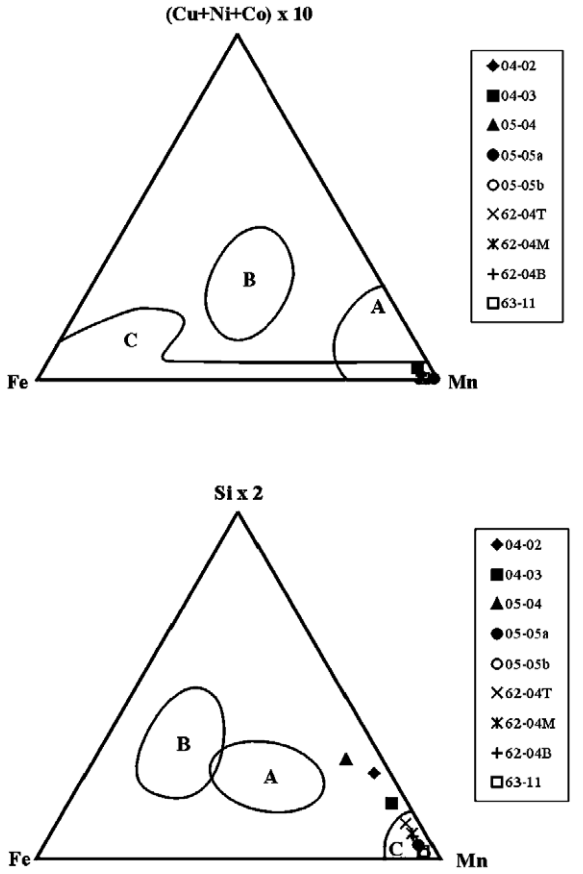

Fig. 5. (Top) Classification of Mn oxide deposits based on Mn–Fe–(Cu+Co+Ni×10) from Baby Bare seamount as (A) diagenetic, (B) hydrogenous (Hein et al., 1992b), or (C) hydrothermal. The diagenetic and hydrothermal fields are after Bonatti et al. (1972). (Bottom) Classification of Mn oxide deposits based on Mn–Fe–Si×2 (Toth, 1980) as (A) diagenetic, (B) hydrogenous, or (C) hydrothermal for samples from Baby Bare seamount.

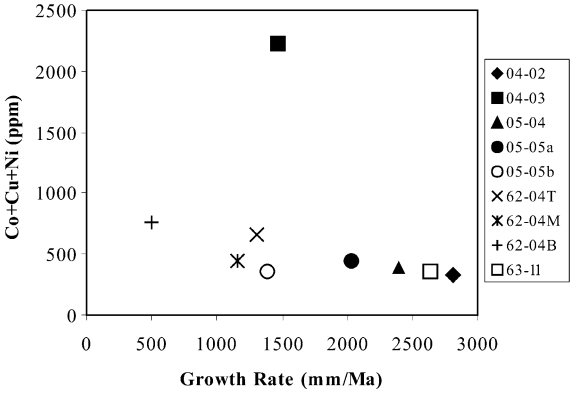

Fig. 6. Comparison of Cu+Co+Ni concentrations (grade) and calculated growth rates in Mn-oxide crusts. With the exception of sample 04-03, there is a correlation (R^2=0.61) between growth rate and grade, showing that the faster the growth rate, the more trace metals are excluded from the Mn crusts.

iment interface (Wheat et al., 2002). This interaction causes a change in redox conditions, which results in the oxidation of Mn^{2+} to MnO_2, which accumulates to form Mn-oxide deposits (Mandernack and Tebo, 1993; Post, 1999 and references therein). 10 Å manganate is an end product of Mn^{2+} oxidation (Golden et al., 1986) and is the primary mineral phase in Mn-oxide crusts from Baby Bare. Trace amounts of authigenic nontronite incorporated during growth with the Mn-oxide phases likely formed as a result of oxidation of Fe^{2+} in the basement (e.g., Alt, 1988). Authigenic nontronite probably formed by a similar process in basal sediments drilled in the Baby Bear area, from upwelling basement fluids (Buatier et al., 2001).

The trace element and REE concentrations of Mn crusts are controlled by adsorption of elements onto MnO_2 surfaces (Toth, 1980), and the growth rates of the crusts. The trace metals (Co, Ni, and Zn) absorbed by the Mn-oxides were primarily derived from the basement component of the spring fluids, as their concentrations are low in seawater. Crusts at Baby Bare with lower trace metal concentrations had faster growth rates (Fig. 6). In contrast, the adsorbed REEs were most likely derived from the seawater component because basement fluids have lower REE contents than seawater (5% to 70%) (Wheat and Mottl, 2002) due to reactions within the volcanic basement (e.g., Porter et al., 2000). Mn-oxide crust REE patterns mimic those of both seawater and spring fluids (Fig. 7). For example, spring fluid La_N/Nd_N (3.0–7.4, average=4.5) and Dy_N/Yb_N ratios (0.6–2.1, average=1.2) overlap those of Mn-oxide crusts (2.7–4.3 and 0.4–1.1, respectively). Mn-oxide Ce anomalies in the Baby Bare crusts range from 0.32 to 0.96. These values are higher than that of seawater (0.08) and more similar to basement fluids (e.g., Spring 17, 0.53; Wheat and Mottl, 2002).

Compositions of the crusts are also controlled by their mineralogy. For example, samples with the highest Ba contents contain minor amounts of authigenic barite. It is feasible that high Ba contents in the other samples reflect the presence of barite in amounts undetectable by XRD, as barite precipitation is favored by mixing of warm Ba-rich fluids with cool sulfate-rich seawater (Monnin et al., 2001). Alternatively, high Ba contents may reflect the partitioning of Ba into the todorokite structure (Usui and Someya, 1997). Spring fluids are enriched in Ba relative to seawater due to reactions in the volcanic basement and sediments along recharge pathways distal from Baby Bare (Monnin et al., 2001).

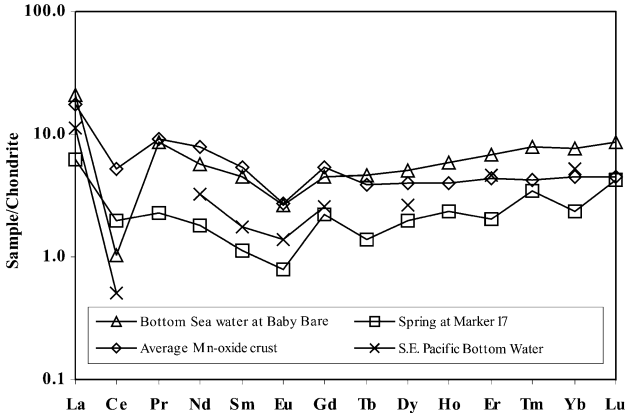

Fig. 7. Chondrite normalized REE plot for average Mn crusts (this study), spring fluids and Baby Bare bottom seawater (Wheat et al., 2003). Data of SE Pacific bottom seawater (2500 m water depth) from Klinkhammer et al. (1983). Fluid values have been multiplied by 1000 to bring values up to the scale of the oxide deposits. Note that sample 62-04B shows a prominent negative Eu anomaly. Eu is below detection limits (0.05 ppm) in the other samples, which suggests that all samples may have negative Eu anomalies.

Finally, the incorporation of clay minerals and other components from the sediment also influences Mn crust compositions. The Si/Al ratios of Mn crusts and the surrounding sediments are similar, suggesting that the primary source of these elements in the crusts is sediment.

6.3. Age and Mn-oxide crust growth rates

It is possible to estimate the rate at which Mn-oxide deposits precipitated using the empirically derived growth equations of Manheim and Lane-Bostwick (1988). Their "cobalt chronometer" for hydrothermal deposits utilizes the concentrations of Fe, Mn, and Co in Mn-oxide crusts to calculate an estimated growth rate. The primary factor that influences Co concentrations in Mn-oxide crusts is the growth rate, since the flux of Co into different types of Mn-oxide crusts is relatively constant (Halbach et al., 1983; Hein et al., 1992b). Co is sorbed onto MnO_2 substrates and is then oxidized from Co(II) to Co(III). A normalized value of Co concentration (in ppm) Co^n, is calculated from the measured concentration of Co, whereby $Co^n = Co \times 50/Fe+Mn$ and Fe+Mn=normalized percent by weight of Fe+Mn. Fe+Mn was chosen as the normalizing factor because Fe and Mn are the building blocks of all oxide crusts and these elements are analyzed in nearly all samples (Manheim and Lane-Bostwick, 1988). The equation $R = 6.8 \times 10^{-1}/(Co^n)^{1.67}$, in mm/Myr, is then used to calculate the growth rate of the Mn crust and has been found to apply consistently for all types of Mn-oxide crusts (Hein et al., 1994). One limitation of the calculation is that the equation does not take into account possible hiatuses in hydrothermal venting. The calculated rates therefore represent maximum values and the derived ages (using sample thicknesses) minimum values (Hein et al., 1990; McMurtry et al., 1994). In general, Th/U ages of other deposits agree well with ages calculated using the cobalt chronometer and the crust thicknesses (Moore and Vogt, 1976; Cronan et al., 1982; Lalou et al., 1983; Bolton et al., 1988; Hodkinson et al., 1994).

Calculated growth rates for Baby Bare crusts range from ~324 to 1800 mm/Myr, consistent with a hydrothermal origin. Maximum crust ages, calculated using the growth rate and thickness for each sample, range from 11,700 to 51,000 yrs (Table 3). From the observed maximum thickness of the outcrop (0.5 m), it is inferred that the age of the deposit age ranges from about 272 to 665 kyrs, with sample 62-04B showing an age of 1.5 Myr. This demonstrates that hydrothermal venting at Baby Bare has taken place at least since 0.5 Myr, and possibly since 1.5 Myr ago. Because these calculated ages are minimum values, it is also possible that Baby Bare has been hydrothermally active since its formation 1.7–2.7 Myr ago.

Table 3
Calculated growth rates[a] and ages[b] for Mn-oxide crusts

Sample no.	Growth rate (mm/Myr)	Sample thickness (mm)	Age–Sample scale (kyr)	Age–Outcrop scale (kyr)
J2-04-02	1800	32	17	272
J2-04-03	960	35	36	520
J2-05-04	1600	80	51	318
J2-05-05A	1300	40	30	377
J2-05-05B	900	40	44	553
62-04T	850	10	12	585
62-04M	750	30	40	665
62-04B	300	10	31	1544
63-11	1700	30	17	290

[a] Growth rates calculated using the empirical equation by Manheim and Lane-Bostwick (1988).
[b] Ages at the sample scale were calculated using the growth rate and individual sample thickness. Ages at the outcrop scale were calculated using the growth rates and observed maximum outcrop thickness of 0.5 m.

The future of hydrothermal venting at Baby Bare seamount is not known, as the impacts of changing variables such as permeability and sediment thickness on fluid flow are difficult to predict. It is reasonable to assume that venting will cease once Baby Bare is completely buried ~0.2 Myr from now based on current sedimentation rates (Davis et al., 1999; Wheat et al., 2004) and may have detectable fluid flow through sediment for an additional 0.5 Myr (Wheat et al., 2004). This demonstrates that the geochemical fluxes associated with warm ridge-flank hydrothermal springs (e.g., Wheat and Mottl, 1994, 2000) have a short-lived impact on global geochemical cycles.

7. Summary

A stratabound, hydrothermal Mn-oxide deposit has been discovered near the summit of Baby Bare seamount, on the eastern flank of the Juan de Fuca Ridge. The seamount is actively venting warm fluids, mixtures of basement fluids and seawater. Manganese oxide crusts are composed primarily of 10 Å manganate ± pyrolusite with minor nontronite, saponite and barite. They have high Mn/Fe ratios, low trace metal and REE contents, strong negative Ce anomalies, and high Ba contents. These chemical characteristics were influenced by spring fluid and seawater chemistry, and bulk mineralogy. Growth rate and age calculations indicate that Baby Bare may have been hydrothermally active

for at least 0.5 Myr and possibly since 1.5 Myr, near the time of its formation (1.7–2.7 Myr ago).

Acknowledgements

The authors thank Chief Scientist H. Paul Johnson for inviting C.E.F. on the LeXeN cruises and the crews of the *R/V Thomas G. Thompson*, *R/V Atlantis* and *ROV Jason-II* for assistance with sample collection. We also graciously thank S. Calvert for XRD analyses, R. Cox for ICP–MS analyses and M. Raudsepp and B. Gowen for assistance with the SEM. Two anonymous reviews helped improve the clarity and focus of this contribution. Natural Sciences and Engineering Research Council Discovery Grant to KMG supported this project.

References

Alt, J.C., 1988. Hydrothermal oxide and nontronite deposits on seamounts in the eastern Pacific. Mar. Geol. 81, 227–239.

Becker, N.C., Wheat, C.G., Mottl, M.J., Karsten, J.L., Davis, E.E., 2000. A geological and geophysical investigation of Baby Bare, locus of a ridge-flank hydrothermal system in the Cascadia Basin. J. Geophys. Res. 105, 23557–23568.

Bolton, B.R., Both, R., Exon, N.F., Hamilton, T.F., Ostwald, J., Smith, J.D., 1988. Geochemistry and mineralogy of seafloor hydrothermal and hydrogenetic Mn oxide deposits from the Manus Basin and Bismarck Archipelago region of the Southwest Pacific Ocean. Mar. Geol. 85, 65–87.

Bonatti, E., Kraemer, T., Rydell, H., 1972. Classification and genesis of submarine iron–manganese deposits. In: Horn, D. (Ed.), Ferromanganese Deposits on the Ocean Floor. National Science Foundation, pp. 149–165.

Buatier, M.D., Monnin, C., Fruh-Green, G.L., Karpoff, A.-M., 2001. Fluid–sediment interactions related to hydrothermal circulation in the Eastern Flank of the Juan de Fuca Ridge. Chem. Geol. 175, 343–360.

Buatier, M.D., Guillaume, D., Wheat, C.G., Herve, L., Adatte, T., 2004. Mineralogical characterization and genesis of hydrothermal Mn oxides from the flank of the Juan the Fuca Ridge. Am. Mineral. 89, 1807–1815.

Calvert, S.E., Price, N.B., 1970. Composition of manganese nodules and manganese carbonates from Loch Fyne, Scotland. Contrib. Mineral. Petrol. 29, 215–233.

Cronan, D.S., Glasby, G.P., Moorby, S.A., Thomson, J., Knedler, K.E., McDougall, J.C., 1982. A submarine hydrothermal manganese deposit from the South-west Pacific Island Arc. Nature 298, 456–458.

Davis, E.E.C., Chapman, D.S., Mottl, M.J., Bentkowski, W.J., Dadey, K., Forster, C., Harris, R., Nagihara, S., Rohr, K., Wheat, G., Whiticar, M., 1992. FlankFlux: an experiment to study the nature of hydrothermal circulation in young oceanic crust. Can. J. Earth Sci. 29, 925–952.

Davis, E.E., Fisher, A.T., Firth, J.V., 1997. Proc. ODP, Init. Repts., vol. 168. Ocean Drilling Program, College Station, TX. 470 pp.

Davis, E.E., Chapman, D.S., Wang, K., Villinger, H., Fisher, A.T., Robinson, S.W., Grigel, J., Pribnow, D., Stein, J., Becker, K., 1999. Regional heat flow variations across the sedimented Juan de Fuca Ridge eastern flank: constraints on lithospheric cooling and lateral hydrothermal heat transport. J. Geophys. Res. 104, 17675–17688.

DeCarlo, E., 1983. Geochemistry of hydrothermal deposits from Loihi submarine volcano, Hawaii. Earth Planet. Sci. Lett. 66, 438–449.

Dulski, P., 1994. Interferences of oxide, hydroxide and chloride analyte species in the determination of rare earth elements in geological samples by inductively coupled plasma–mass spectrometry. J. Anal. Chem. 350, 194–203.

Eckhardt, J.-D., Glasby, G.P., Puchelt, H., Berner, Z., 1997. Hydrothermal manganese crusts from Enarete and Palinuro seamounts in the Tyrrhenian Sea. Mar. Georesour. Geotechnol. 15, 175–208.

Elderfield, H., Schultz, A., 1996. Mid-ocean ridge hydrothermal fluxes and the chemical composition of the ocean. Annu. Rev. Earth Planet. Sci. 24, 191–224.

Fisher, A.T., Davis, E.E., Hutnak, M., Spiess, V., Zuhlsdorff, L., Cherkaoul, A., Christiansen, L., Edwards, K., MacDonald, R., Villinger, H., Mottl, M.J., Wheat, C.G., Becker, K., 2003. Hydrothermal recharge and discharge across 50 km guided by seamounts on a young ridge flank. Nature 421, 618–621.

Golden, D.C., Chen, C.C., Dixon, J.B., 1986. Synthesis of todorokite. Science 231, 717–719.

Grill, E.V., Chase, R.L., MacDonald, R.D., Murray, J.W., 1981. A hydrothermal deposit from Explorer Ridge in the Northeast Pacific Ocean. Earth Planet. Sci. Lett. 52, 142–150.

Halbach, P., Segl, M., Puteanus, D., Arrhenius, G., 1983. Co-fluxes and growth rates in ferromanganese deposits from central Pacific seamounts. Nature 304, 716–718.

Halbach, P., Sattler, C.-D., Teichmann, F., Wahsner, M., 1989. Cobalt-rich and platinum-bearing manganese crust deposits on seamounts: nature, formation, and metal potential. Mar. Min. 8, 23–39.

Hein, J.R., Schulz, M.S., Kang, J.-K., 1990. Insular and submarine ferromanganese mineralization of the Tonga–Lau region. Mar. Min. 9, 305–354.

Hein, J.R., Ahn, J.H., Wong, J.C., et al., 1992a. Geology, geophysics, geochemistry, and deep-sea mineral deposits. Federated States of Micronesia: KORDI-USGS *R.V. Farnella cruise* F11-90-CP. U.S.G.S. Open File Rept., pp. 92–218.

Hein, J.R., Schulz, M.S., Gein, L.M., 1992b. Central Pacific cobalt-rich ferromanganese crusts: historical perspective and regional variability. In: Keating, B.H., Bolton, B.R. (Eds.), Geology and Offshore Mineral Resources of the Central Pacific Basin. Springer-Verlag, Berlin, pp. 261–283.

Hein, J.R., Yeh, H.-W., Gunn, S.H., Gibbs, A.E., Wang, C.-H., 1994. Composition and origin of hydrothermal ironstones from central Pacific seamounts. Geochim. Cosmochim. Acta 58, 179–189.

Hein, J.R., Gibbs, A.E., Clague, D., Torresan, M., 1996. Hydrothermal mineralization along submarine rift zones, Hawaii. Mar. Georesour. Geotechnol. 14, 177–2003.

Hein, J.R., Kochinsky, A., Halbach, P., Manheim, F.T., Bau, M., Kang, J.-K., Lubick, N., 1997. Iron and manganese oxide mineralization in the Pacific. In: Nicholson, K., Hein, J.R., Buhn, B., Dasgupta, S. (Eds.), Manganese Mineralization: Geochemistry and Mineralogy of Terrestrial and Marine Deposits, Geol. Soc. Lond. Spec. Publ., vol. 119, pp. 123–138.

Herzig, P.M., Von Stackelberg, U., Petersen, S., 1990. Hydrothermal mineralization from the Valu Fa Ridge, Lau Back-Arc basin (SW Pacific). Mar. Min. 9, 271–301.

Hodkinson, R.A., Stoffers, P., Scholten, J., Cronan, D.S., Jeschke, G., Rogers, T.D.S., 1994. Geochemistry of hydrothermal manganese deposits from the Pitcairn Island hotspot, southeastern Pacific. Geochim. Cosmochim. Acta 58, 5011–5029.

Honnorez, J., Karpoff, A.-M., Trauth-Badaut, D., 1983. Sedimentology, mineralogy, and geochemistry of green clay samples from the Galapagos hydrothermal mounds, Holes 506, 506C, and 507D, Deep Sea Drilling Project Leg 70 (preliminary data). In: Honnorez, J., Von Herzen, R.P., et al., (Eds.), Init. Rep. Deep Sea Drill. Proj. U.S. Gov. Printing Office, Washington, DC, pp. 211–220.

Ingram, B.L., Hein, J.R., Farmer, G.L., 1990. Age determinations and growth rates of Pacific ferromanganese deposits using strontium isotopes. Geochim. Cosmochim. Acta 54, 1709–1721.

Johnson, unpublished cruise report, 2002. Collaborative Lexen Research: Direct Sampling of the Oceanic Subsurface Biosphere at Old and Young Seamounts. 366 pp.

Johnson, H.P., 2003. Probing for life in the ocean crust with the LEXEN program. EOS Trans. Amer. Union, 84, 109, 112.

Kappel, E.S., Ryan, W.B.F., 1986. Volcanic episodicity and a non-steady state rift-valley along Northeast Pacific spreading centers—evidence from Sea Marc-1. J. Geophys. Res. 91, 13925–13940.

Klinkhammer, G.P., Heggie, D.T., Graham, D.W., 1982. Metal diagenesis in oxic marine sediments. Earth Planet. Sci. Lett. 61, 211–219.

Klinkhammer, G.P., Elderfield, H., Hudson, A., 1983. Rare earth elements in seawater near hydrothermal vents. Nature 305, 185–188.

Kuhn, T., Bau, M., Blum, N., Halbach, P., 1998. Origin of negative Ce anomalies in mixed hydrothermal–hydrogenetic Fe–Mn crusts from the Central Indian Ridge. Earth Planet. Sci. Lett. 163, 207–220.

Lalou, C., 1983. Genesis of ferromanganese deposits: hydrothermal origin. In: Rona, P.A., Böstrom, K., Laubier, L., Smith Jr., K.L. (Eds.), Hydrothermal Processes at Seafloor Spreading Centers. NATO Conference Series IV: Marine Sciences. Plenum Press, New York, pp. 503–534.

Lalou, C., Brichet, E., Jehanno, C., Perez-Leclaire, H., 1983. Hydrothermal manganese oxide deposits from Galapagos mounds, DSDP Leg 70, Hole 509B and Alvin dives 729 and 721. Earth Planet. Sci. Lett. 63, 63–75.

Mandernack, K.W., Tebo, B.M., 1993. Manganese scavenging and oxidation at hydrothermal vents and in vent plumes. Geochim. Cosmochim. Acta 57, 3907–3923.

Manheim, F.T., Lane-Bostwick, C.M., 1988. Cobalt in ferromanganese crusts as a monitor of hydrothermal discharge on the Pacific seafloor. Nature 335, 59–62.

McMurtry, G.M., Vonderhaar, D.L., Eisenhauer, A., Mahoney, J.J., Yeh, H.W., 1994. Cenozoic accumulation history of a Pacific ferromanganese crust. Earth Planet. Sci. Lett. 125, 105–118.

Monnin, C., Wheat, C.G., Dupre, B., Elderfield, H., Mottl, M.J., 2001. Barium geochemistry in sediment pore waters and formation waters of the oceanic crust on the eastern flank of the Juan de Fuca Ridge (ODP Leg 168). Geochem. Geophys. Geosyst. 2, 1–19.

Moore, W.S., Vogt, P.R., 1976. Hydrothermal manganese crusts from two sites near the Galapagos spreading axis. Geochim. Cosmochim. Acta 29, 349–356.

Mottl, M.J., 2002. Partitioning of energy and mass fluxes between mid-ocean ridge axes and flanks at high and low temperature. In: Halbach, P.E., Tunnicliffe, V., Hein, J.R. (Eds.), Dahlem Workshop on Energy and Mass Transfer in Marine Hydrothermal Systems. Freie Universitat Berlin, Berlin, Germany, pp. 271–286.

Mottl, M.J., Wheat, C.G., 1994. Hydrothermal circulation through mid-ocean ridge flanks: fluxes of heat and magnesium. Geochim. Cosmochim. Acta 58, 2225–2237.

Mottl, M.J., Wheat, C.G., Baker, E., Becker, N., Davis, E., Feely, R., Grehan, A., Kadko, D., Lilley, M., Massoth, G., Moyer, C., Sansone, F., 1998. Warm springs discovered on 3.5 Ma oceanic crust, eastern flank of the Juan de Fuca Ridge. Geology 26, 51–54.

Porter, S., Vanko, D.A., Ghazi, A.M., 2000. Major and trace element compositions of secondary clays in basalts altered at low temperature, eastern flank of the Juan de Fuca Ridge. In: Fisher, A.T., Davis, E.E., Escutia, C. (Eds.), Proc. ODP Sci. Results, vol. 168. Ocean Drilling Program, College Station, TX, pp. 149–157.

Post, J.E., 1999. Manganese oxide minerals: crystal structures and economic and environmental significance. Proc. Natl. Acad. Sci. U. S. A. 96, 3447–3454.

Stein, C.A., Stein, J.S., 1994. Constraints on hydrothermal heat flux through the oceanic lithosphere from global heat flow. J. Geophys. Res. 99, 3081–3095.

Sun, S.-S., McDonough, W.F., 1989. Chemical and isotopic systematics of oceanic basalts: implications for mantle composition and processes. In: Saunders, A.D., Norry, M.J. (Eds.), Magmatism in the Ocean Basins. Geol. Soc. London, Spec. Pub., London, UK, pp. 313–345.

Taylor, V.F., Toms, A., Longerich, H.P., 2002. Acid digestion of geological and environmental samples using open-vessel focused microwave digestion. Anal. Bioanal. Chem. 372, 360–365.

Toth, J.R., 1980. Deposition of submarine crusts rich in manganese and iron. Geol. Soc. Amer. Bull. 91, 44–54.

Underwood, M.B., Hoke, K.D., 2000. Composition and provenance of turbidite sand and hemipelagic mud in Northwestern Cascadia Basin. In: Fisher, A., Davis, E., Escutia, C. (Eds.), Proc. ODP Sci. Results, vol. 168. Ocean Drilling Program, College Station, TX, pp. 51–65.

Usui, A., Nishimura, A., 1992. Submersible observations of hydrothermal manganese deposits on the Kaikata Seamount, Izu-Ogasawara (Bonin). Arc. Mar. Geol. 106, 203–216.

Usui, A., Someya, M., 1997. Distribution and composition of marine hydrogenetic and hydrothermal manganese deposits in the northwest Pacific. In: Nicholson, K., Hein, J.R., Buhn, B., Dasgupta, S. (Eds.), Manganese Mineralization: Geochemistry and Mineralogy of Terrestrial and Marine Deposits, Geol. Soc. of Lond. Spec. Publ., vol. 119, pp. 177–198.

Usui, A., Yuasa, M., Yokota, M., Nishimura, A., Murakami, F., 1986. Submarine hydrothermal manganese deposits from the Ogasawara (Bonin) Arc, off the Japan Islands. Mar. Geol. 73, 311–322.

Varentsov, I.M., Drits, V.A., Gorshkoz, A.I., Sivtsov, A.V., Sakharov, B.A., 1991. Mn–Fe oxyhydroxide crusts from Krylov Seamount (eastern Atlantic): mineralogy, geochemistry and genesis. Mar. Geol. 96, 53–70.

Varnavas, S.P., Papaioannou, J., Catani, J., 1988. A hydrothermal manganese deposit from the Eratosthenes Seamount, eastern Mediterranean Sea. Mar. Geol. 81, 205–214.

Villinger, H., Grevenmeyer, I., Kaul, N., Hauschild, J., Pfender, M., 2002. Hydrothermal heat flux through aged ocean crust: where does the heat escape? Earth Planet. Sci. Lett. 202, 159–170.

Wessel, P., 2001. Global distribution of seamounts inferred from gridded Geosat/ERS-1 altimetry. J. Geophys. Res. 106, 19431–19441.

Wheat, C.G., McDuff, R.E., 1995. Hydrothermal flow through the Mariana Mounds: dissolution of amorphous silica and degradation

of organic matter on a mid-ocean ridge flank. Geochim. Cosmochim. Acta 58, 2461–2475.

Wheat, C.G., Mottl, M.J., 1994. Hydrothermal circulation, Juan de Fuca Ridge eastern flank: factors controlling basement water composition. J. Geophys. Res. 99, 3067–3080.

Wheat, C.G., Mottl, M.J., 2000. Composition of pore and spring waters from Baby Bare: global implications of geochemical fluxes from a ridge flank hydrothermal system. Geochim. Cosmochim. Acta 64, 629–642.

Wheat, C.G., Elderfield, H., Mottl, M.J., Monnin, C., 2000. Chemical composition of basement fluids within an oceanic ridge flank: implications for along-strike and across-strike hydrothermal circulation. J. Geophys. Res. 105, 13437–13447.

Wheat, C.G., Mottl, M.J., Rudnicki, M., 2002. Trace element and REE composition of a low-temperature ridge-flank hydrothermal spring. Geochim. Cosmochim. Acta 66, 3693–3705.

Wheat, C.G., Jannasch, H.W., Kastner, M., Plant, J.N., De Carlo, E.H., 2003. Seawater transport and reaction in upper oceanic basaltic basement: chemical data from continuous monitoring of sealed boreholes in a ridge flank environment. Earth Planet. Sci. Lett. 216, 549–564.

Wheat, C.G., Mottl, M.J., Fisher, A.T., Kadko, D., Davis, E.E., Baker, E., 2004. Heat flow through a basaltic outcrop on a sedimented young ridge flank. Geochem. Geophys. Geosyst. 5, Q12006. doi:10.1029/2004GC000700.